NIH Public Access
Author Manuscript
J Nucl Med. Author manuscript; available in PMC 2014 July 30.

Published in final edited form as:
J Nucl Med. 2014 May ; 55(5): 799–804. doi:10.2967/jnumed.113.132118.

Glypican-3–Targeted ^{89}Zr PET Imaging of Hepatocellular Carcinoma

Jonathan G. Sham[1], **Forrest M. Kievit**[2], **John R. Grierson**[3], **Robert S. Miyaoka**[3], **Matthew M. Yeh**[4], **Miqin Zhang**[5], **Raymond S. Yeung**[1], **Satoshi Minoshima**[3], and **James O. Park**[1]

[1]Department of Surgery, University of Washington, Seattle, Washington

[2]Department of Neurosurgery, University of Washington, Seattle, Washington

[3]Department of Radiology, University of Washington, Seattle, Washington

[4]Department of Pathology, University of Washington, Seattle, Washington

[5]Department of Materials Science and Engineering, University of Washington, Seattle, Washington

Abstract

Hepatocellular carcinoma (HCC) is a devastating malignancy in which imperfect imaging plays a primary role in diagnosis. Glypican-3 (GPC3) is an HCC-specific cell surface proteoglycan overexpressed in most HCCs. This paper presents the use of ^{89}Zr-conjugated monoclonal antibody against GPC3 (^{89}Zr-αGPC3) for intrahepatic tumor localization using PET.

Methods—Polymerase chain reaction confirmed relative GPC3 expression in cell lines. In vitro binding, in vivo biodistribution, and small-animal PET studies were performed on GPC3-expressing HepG2 and non–GPC3-expressing HLF and RH7777 cells and orthotopic xenografts.

Results—^{89}Zr-αGPC3 demonstrated antibody-dependent, antigen-specific tumor binding. HepG2 liver tumors exhibited high peak uptake (836.6 ± 86.6 percentage injected dose [%ID]/g) compared with background liver (27.5 ± 1.6 %ID/g). Tumor-to-liver contrast ratio was high and peaked at 32.5. The smallest HepG2 tumor (<1 mm) showed lower peak uptake (42.5 ± 6.4 %ID/g) and tumor-to-liver contrast (1.57) but was still clearly visible on PET. Day 7 tissue activity was still substantial in HepG2 tumors (466.4 ± 87.6 %ID/g) compared with control RH7777 tumors (3.9 ± 1.3 %ID/g, $P < 0.01$), indicating antigen specificity by ^{89}Zr-αGPC3. HepG2 tumor treated with unlabeled αGPC3 or heat-denatured ^{89}Zr-αGPC3 demonstrated tumor activity (2.1 %ID/g) comparable to that of control xenografts, confirming antibody dependency.

Conclusion—This study demonstrated the feasibility of using ^{89}Zr-αGPC3 to image HCC in the liver, as well as the qualitative determination of GPC3 expression via small-animal PET. The ability to clarify the identity of small liver lesions with an HCC-specific PET probe would provide

© 2014 by the Society of Nuclear Medicine and Molecular Imaging, Inc.

For correspondence or reprints contact: James O. Park, 1959 N.E. Pacific St., Box 356410, Seattle, WA 98195-6410. jopark@uw.edu.

DISCLOSURE
Financial support was received from NCI grant T32CA138312 and a University of Washington Department of Surgery reinvestment grant. The content is solely the responsibility of the authors and does not necessarily represent the official views of the NCI or NIH. No other potential conflict of interest relevant to this article was reported.

NIH-PA Author Manuscript
NIH-PA Author Manuscript
NIH-PA Author Manuscript

NIH-PA Author Manuscript

NIH-PA Author Manuscript

NIH-PA Author Manuscript

clinicians with vital information that could significantly alter patient management, warranting further investigation for clinical translation.

Keywords

hepatocellular carcinoma; ^{89}Zr; glypican 3; liver; PET

With more than 782,000 new cases and 746,000 resultant deaths annually, hepatocellular carcinoma (HCC) is the fifth most prevalent malignancy and the second leading cause of cancer-related deaths worldwide (1,2). High-quality, accurate imaging is an essential component in the detection, staging, and treatment planning of HCC, wherein subtle findings can dramatically alter the management plan (3,4). Multiphase contrast-enhanced CT or MR imaging is the current gold standard, with HCC tumors classically demonstrating late arterial enhancement with portal venous washout, obviating tissue diagnosis (3–5). However, CT and MR scans frequently detect lesions that cannot be further defined, introducing uncertainty about the diagnosis or disease extent (4–7). Comparison of liver tumor enhancement patterns at various time points after intravenous contrast administration to distinguish benign entities from HCC is limited by lack of specificity (4,6). This problem is further exacerbated by institutional variability in protocols defining the type, dosage, and timing of intravenous contrast material (7). As scan sensitivity improves, an increasing number of such indeterminate lesions are detected. Doubt raised by these lesions triggers costly repeated imaging, or biopsy with bleeding or tumor-seeding risks (8,9), all contributing to delayed treatment of these patients. Furthermore, basing eligibility for potentially curative liver resection or transplantation on suboptimal scans leads to either early recurrences or missed treatment opportunities. Studies comparing tumor extent on preoperative imaging with liver explant pathology have demonstrated a troubling discordance (10), and most relapses after curative treatment occur within 2 y (11,12), reflecting subclinical disease missed at the time of initial radiographic diagnosis, both highlighting the inaccuracy of current imaging.

Targeted molecular imaging addresses many limitations presented by conventional diagnostic approaches. ^{89}Zr has recently emerged as a promising PET radioisotope when targeted with monoclonal antibodies (mAbs) (13,14), and conjugation of ^{89}Zr to several preclinical and clinically available mAbs has demonstrated high spatial resolution and excellent signal-to-noise ratios (15–17). Reports of antibody-labeled ^{64}Cu and ^{86}Y (half-life, 12.7 and 14.7 h, respectively) have shown promise (18–20). However, the location of HCC in the liver, a primary clearance organ with relatively high background radioisotope uptake, compels use of a highly specific targeting ligand and a longer-half-life radionuclide. ^{89}Zr possesses a far more optimal half-life (78.4 h), allowing unwanted background signal to clear so that the liver tumor can be visualized.

Although under investigation, antibody-based biologic therapy is currently not part of standard HCC treatments (21); therefore, mAbs are not commercially available and novel targeting moieties must be used for PET imaging. Glypican-3 (GPC3) is a heparan sulfate proteoglycan important in regulating embryonal cell growth (22). It is an ideal target because of its overexpression in up to 80% of HCCs and absence in normal tissues, cirrhotic

NIH-PA Author Manuscript

NIH-PA Author Manuscript

NIH-PA Author Manuscript

liver, and benign lesions (23–25). A membrane-bound proteoglycan, it is readily accessible to antibody-mediated targeting, and immunohistochemical GPC3 staining has demonstrated 97% specificity (24–26). Previous experience using our αGPC3 mAb has demonstrated its efficacy as a targeting moiety for MR imaging (27).

Herein we report the development of ^{89}Zr-αGPC3 as a PET contrast agent to identify GPC3-expressing tumors and to serve as an adjunct to multiphase CT and MR in HCC imaging. To our knowledge, this is the first report of mAb-targeted ^{89}Zr-PET in HCC and is the proof-of-concept study for immuno-PET imaging of primary liver tumors.

MATERIALS AND METHODS

Cell Lines and Tissue Culture

Luciferase-expressing GPC3-positive HepG2 HCC cells were purchased from PerkinElmer (Bioware HT1080-luc2), GPC3-negative HLF cells were acquired from the Japanese Cancer Research Resources Bank, and GPC3-negative RH7777 cells were purchased from American Type Culture Collection (ATCC no. CRL-1601). Details are found in the supplemental data (available at http://jnm.snmjournals.org).

Production of αGPC3 IgG1 and ^{89}Zr-Labeled αGPC3

αGPC3 IgG1-producing hybridomas were generated using previously described methods (28) through the Fred Hutchison Cancer Research Center antibody core. ^{89}Zr-αGPC3 labeling was performed by an adaptation of the protocol of Vosjan et al. (29) not requiring extraordinary trace demetalation of materials. Details are found in the supplemental data.

In Vitro Studies

For in vitro evaluation of ^{89}Zr-αGPC3 binding, 2×10^6 HepG2 and HLF were each plated in 60-mm culture dishes (Fisher Scientific) and attached overnight. The cells were treated with ^{89}Zr-αGPC3 (~18.5 MBq/mg of αGPC3) at antibody masses of 1 μg (n = 3), 100 μg (n = 3), and 250 μg (n = 1). To evaluate antibody-dependent cell binding, 2×10^6 cells at the 1 μg (n = 3) and 100 μg (n = 3) conditions were cotreated with 1 mg of unlabeled αGPC3 as a competition assay, and an additional 250-μg (n = 1) ^{89}Zr-αGPC3 sample was heat-denatured by boiling for 5 min before cell treatment. Cells were treated with ^{89}Zr-αGPC3 in 2 mL of Dulbecco modified Eagle medium plus 10% fetal bovine serum for 1 h at room temperature. The cells were washed thrice with 5 mL of phosphate-buffered saline to remove unbound ^{89}Zr-αGPC3 and were subsequently lysed with 0.1% Triton X-100 (Sigma). Lysate radioactivity was measured with a Cobra II auto γ counter (Packard).

Animal Models

All animal studies were performed in accordance with the University of Washington Office of Animal Welfare guidelines for the humane use of animals, and all procedures were reviewed and approved by the Institutional Animal Care and Use Committee. For the orthotopic xenograft model, 8-wk-old female athymic Nu/J mice (Jackson Laboratories) were anesthetized using 1.5% inhaled isoflurane and the left lobe of the liver was exposed through an upper midline laparotomy. HCC cells (2×10^6) in 50 μL of Dulbecco modified

NIH-PA Author Manuscript

NIH-PA Author Manuscript

NIH-PA Author Manuscript

Eagle medium containing 50% Matrigel (BD Biosciences) were injected into the subcapsular space of the left lobe. Four weeks after HepG2 cell injection and 2 wk after RH7777 cell injection, a 75 mg/kg intraperitoneal injection of VivoGlo luciferin (Promega) was administered and imaging was performed using an IVIS Lumina II system (PerkinElmer) to monitor the growth of intrahepatic tumors.

Small-Animal PET

Imaging studies were performed using the Inveon PET scanner (Siemens). Whole-body imaging was performed on mice on a temperature-controlled bed, anesthetized with 1.5%–2.5% isoflurane with real-time respiratory monitoring. Tumor-bearing mice selected by IVIS imaging were injected with approximately 11.1 MBq (300 μCi) of ^{89}Zr-αGPC3 (~70 μg of antibody) via the tail vein. Control animals (n = 4) were coinjected with 1–1.2 mg of unlabeled αGPC3 as a blocking study. In an additional HepG2-bearing animal, the ^{89}Zr-αGPC3 conjugate was boiled for 5 min before injection as a heat-denatured control. Imaging times were as follows: day 0, 30 min; day 1, 30 min; day 3, 60 min; day 5, 80 min; and day 7, 120 min. Details may be found in the supplemental data.

Biodistribution

All animals were injected with approximately 11.1 MBq of ^{89}Zr-αGPC3 (~70 μg of antibody) via the tail vein. Tissue biodistribution was determined in non–tumor-bearing animals 1, 3, 5, and 7 d after injection (n = 4 each). Select HepG2 (n = 7) and RH7777 (n = 4) orthotopic-tumor–bearing mice used for PET imaging were also evaluated on day 7. Four additional HepG2-bearing mice were coinjected with 1–1.2 mg of unlabeled αGPC3 as blocked controls. An additional HepG2-bearing mouse was treated with ^{89}Zr-αGPC3 that had been boiled for 5 min to denature the targeting antibody. At designated times, animals were euthanized and the whole body was perfused with 50 mL of lactated Ringer solution as previously described (30). Tumor, blood, and selected organs were harvested and wet-weighed, and radioactivity was measured using a Cobra II auto γ counter channeled for 0.908 MeV γ (100%) rays. Immunofluorescence and immunohistochemistry were then performed on selected samples to evaluate for the presence of αGPC3 in tumor tissue. PET biodistribution mean activity data were obtained using a 0.02-cm^2 circular ROI with 596.3-μm slice thickness. Measurements were taken in standardized locations in each organ: apex of heart, right upper lobe of lung, right lobe of liver, right superior pole of kidney, right frontal lobe of brain, and a mid-thoracic vertebra. Tumor measurements were taken using the same-sized ROI over the portion of the tumor with the highest activity. Details are found in the supplemental data.

Statistical Analysis

All numeric data are expressed as median ± SD unless otherwise indicated. Excel (version 12.3.6; Microsoft) was used for statistical analysis. An unpaired, 2-tailed Student t test was used, with a P value of less than 0.05 considered statistically significant.

NIH-PA Author Manuscript

NIH-PA Author Manuscript

NIH-PA Author Manuscript

RESULTS

Differential GPC3 Expression

Evaluation of messenger RNA levels using 2 nonoverlapping primer pairs confirmed significant overexpression of GPC3 in HepG2 compared with HLF and RH7777 cells (Fig. 1). Average normalized fold-expression of GPC3 messenger RNA was markedly elevated using both GPC3-250 (18.8 ± 4.16) and GPC3-430 (17.2 ± 1.8) primer pairs in HepG2 cells when compared with HLF (undetectable) and RH7777 (undetectable) ($n = 3$, $P < 0.01$). These results are consistent with previously reported expression profiles (24).

Radiochemistry

Overall, 98% of the reaction activity (7.5 mL) was recovered from the reaction mixture and rinses applied to the purification PD-10 column. A heart-cut of fractions with maximal activity was pooled and sterilized by micron filtration (4.26 mCi [158 MBq]; 59% radiochemical yield; >96% specifically bound activity by instant thin-layer chromatography). Analytic size-exclusion chromatography and high-performance liquid chromatography analysis (phosphate-buffered saline, pH 7.4; Superdex-200 10/300 GL; GE Healthcare) showed that the labeled antibody was highly homogeneous and coeluted with the native αGPC3 antibody standard. The specific activity of the labeled antibody was 0.16 GBq/mg (4.2 mCi/mg), assuming 85% protein recovery from the column. The formulated dose was subsequently used for small-animal PET studies on tumor-bearing mice.

In Vitro Evaluations

^{89}Zr-αGPC3 demonstrated antibody-dependent, antigen-specific cell binding in vitro (Fig. 2). The radiotracer signal in the cell lysate was markedly increased in the 1-, 100-, and 250-μg treatment conditions. The average radioactivity of the 250-μg treatment condition was similar to that of 100 μg (3,377.5 vs. 3,791.6 ± 119.1 Bq/million cells), suggesting membrane antigen saturation at this level. Blocking of the 1- and 100-μg conditions with 1 mg of unlabeled αGPC3 reduced radioactivity by 68- and 34-fold, respectively. Likewise, the heat-denatured 250-μg condition reduced radiotracer binding 44-fold. Treatment of GPC3-negative HLF cells with 100 μg of ^{89}Zr-αGPC3 yielded low radiotracer signal (65.0 ± 6.6 Bq/million cells) indicating minimal cell binding, significantly lower than blocked HepG2 cells treated with the same radioisotope dose (108.3 ± 12.6 Bq/million cells, $P < 0.01$).

Tissue Biodistribution Studies

In vivo tissue biodistribution was evaluated 1, 3, 5, and 7 d after administration of ^{89}Zr-αGPC3 (Fig. 3). Tissue uptake was highest in the kidneys, peaking on day 5 (33.4 ± 7.9 percentage injected dose [%ID]/g) and falling to 23.8% ± 3.6% by day 7. Blood-pool activity fell 2.5-fold from 16.6 ± 2.1 %ID/g on day 1 to 6.5 ± 3.0 %ID/g on day 7. Liver uptake peaked at 20.8 ± 5.3 %ID/g on day 3 and fell to 13.5 ± 1.7 %ID/g on day 7. Tissue uptake in the bone, brain, cecum, heart, lungs, and muscle remained below 5 %ID/g throughout the duration of the study.

NIH-PA Author Manuscript

NIH-PA Author Manuscript

NIH-PA Author Manuscript

Tumor size-matched animals in the HepG2, RH7777, and HepG2-blocked groups demonstrated comparable tissue uptake in clearance organs at day 7 (Fig. 4). No statistical difference existed in kidney, liver, and splenic uptake between these groups (all P values > 0.05). Tumor uptake was 121-fold higher in HepG2 animals than in RH7777 controls (466.4 ± 87.6 %ID/g vs. 3.9 ± 1.3 %ID/g, $P < 0.01$). Additionally, tumor uptake was 16-fold lower in animals coinjected with unlabeled αGPC3 than in unblocked animals (29.0 ± 8.6 %ID/g vs. 466.4 ± 87.6 %ID/g), further confirming the antigen dependency of ^{89}Zr-αGPC3 binding.

In the HepG2 tumor-bearing animal injected with heat-denatured ^{89}Zr-αGPC3, kidney activity (22.3 %ID/g) was similar to that in non–heat-denatured HepG2 and HepG2 blocked animals. However, as the result of aggregation during heat denaturing, large-molecule clearance organs including liver and spleen showed a marked increase in activity (42.7 and 305.4 %ID/g, respectively). Heat-denaturing ^{89}Zr-αGPC3 appeared to eliminate liver tumor binding in a size-matched HepG2 tumor-bearing control animal, as activity in this mouse's tumor (2.1 %ID/g) was similar to that in RH7777 negative controls and markedly lower than that in HepG2 tumors when the radioconjugate was not denatured.

Small-Animal PET Imaging

Day 7 tissue activity was compared between the small-animal PET data and Cobra II γ-counter measurements from the same animals (Supplemental Fig. 1). There was a slight trend toward increased measured activity in the PET images, likely due to blood-pool activity that is removed by whole-animal perfusion before γ-counter measurements. However, no statistical difference was found when PET and γ-counter activity were compared across 6 different organs.

Given this concordance, small-animal PET measurements of the liver and liver tumor were obtained at multiple time points in 2 animals with different-sized tumors as determined by histology: 3.8 mm versus less than 1 mm (Fig. 5). For the larger tumor, average tumor uptake peaked on day 3 (836.6 ± 86.6 %ID/g) and fell to its lowest point on day 7 (443.9 ± 80.5 %ID/g). Background liver activity fell by half (27.5 ± 1.6 %ID/g to 13.7 ± 0.6 %ID/g), leading to gradually increasing tumor-to-liver uptake ratios peaking on day 7 at 32.5 despite a nearly 50% drop in tumor %ID/g. The animal with the smaller tumor demonstrated an overall lower average tumor uptake that was highest on day 1 (42.5 ± 6.4 %ID/g) and fell to its lowest point on day 7 (21.6 ± 3.5 %ID/g). Background liver activity was virtually identical to that in the larger-tumor animal, starting at 27.1 ± 1.7 %ID/g on day 1 and falling to 14.4 ± 0.6 %ID/g on day 7. Given the overall lower tumor activity and similar liver activity in this animal, the tumor-to-liver ratio was significantly smaller but remained relatively stable over the course of the experiment, ranging from 1.57 to 1.49.

Histology

Serial hematoxylin and eosin sections of the larger HepG2 tumor (by PET) revealed a maximum diameter of 3.8 mm. The smaller HepG2 tumor could not be visualized histologically by a board-certified liver pathologist after serial sectioning of the left lobe of the liver, likely because of technical considerations regarding the sectioning and staining

NIH-PA Author Manuscript

NIH-PA Author Manuscript

NIH-PA Author Manuscript

procedure, as well as the diminutive size of the tumor. Given its appearance relative to the larger tumor on PET and IVIS imaging, we estimate its size at less than 1 mm.

Immunohistochemistry against GPC3 confirmed polymerase chain reaction data illustrating high expression in HepG2 and minimal expression in RH7777, as well as demonstrating preservation of relative GPC3 expression profiles after tumor formation (Fig. 6). Using a Cy5.5-conjugated goat antimouse IgG1 for immunofluorescence in HepG2 (human) and RH7777 (rat) liver tumors allowed visualization of mouse anti-human αGPC3 in PET-imaged animal tissues. Immunofluorescence results were consistent with PET and Cobra data, demonstrating high delivery in HepG2 tumors and minimal uptake in RH7777 tumors.

DISCUSSION

High-quality imaging plays a critical role in diagnosis and therapeutic planning for HCC patients. Limitations in both the sensitivity and the specificity of conventional contrast-enhanced, timing-dependent multiphase CT and MR drive the need for molecularly targeted imaging probes to more accurately define indeterminate lesions. In this proof-of-concept study, ^{89}Zr was conjugated to a highly selective mAb against the HCC-specific cell surface proteoglycan GPC3 to create an immuno-PET probe capable of identifying GPC3-expressing tumors in vivo.

^{89}Zr-αGPC3 demonstrated excellent specificity, as indicated by robust cell binding in GPC3-expressing HepG2 tumors and minimal uptake in non–GPC3-expressing RH7777 tumors of greater size. Larger RH7777 tumors were intentionally chosen to maximize the binding opportunity created by the enhanced permeability and retention effect. Cotreatment with an excess of unlabeled αGPC3 significantly reduced tumor uptake to a level equivalent to that in the liver. Additionally, heat denaturing of the ^{89}Zr-αGPC3 limited binding in size-matched HepG2 tumors to levels less than in the negative control RH7777 tumors, further confirming the necessity of αGPC3 mAb for tumor targeting. The substantial increase in liver and splenic activity in the heat-denatured animal is due to the well-known phenomenon of antibody aggregation when subjected to increased tem-which leads to an increase in size (31) and uptake by large-molecule clearance organs. αGPC3 was created using human GPC3 protein and demonstrated high-affinity binding during development. However, binding to other members of the glypican family is still possible and must be considered. Despite this potential, GPC3 shares only 43% sequence homology with GPC5, the next most similar glypican (32). Additionally, other proteoglycans have been studied in both humans and in vitro cell lines, and GPC3 is the only member of the glypican family reported to be overexpressed in HCC (33,34).

Both conceptual and technical concerns have been raised about the use of ^{89}Zr-labeled mAb in liver imaging, because of the variable antigen expression profile of the organ and its native clearance function (16). Despite these challenges, this study represents the first use of mAb-labeled ^{89}Zr to identify a primary liver malignancy. Tumors smaller than 4 mm demonstrated substantial PET signal, and even much smaller tumors (<1 mm) were able to overcome background liver activity to be identified on ^{89}Zr-PET (Fig. 5). Comparisons of activity were drawn between the tumor and liver, rather than blood pool, given that

NIH-PA Author Manuscript

NIH-PA Author Manuscript

NIH-PA Author Manuscript

background liver uptake most directly affects intrahepatic tumor visualization for primary HCC on PET.

In animals bearing larger HepG2 tumors (~4 mm), ^{89}Zr-αGPC3 exhibited remarkably high radiotracer uptake throughout the experiment, with day 7 tissue uptake (%ID/g) approximately $\log_{10}$-fold higher than xenografts in other published reports (16,17). We suspect this finding is due to several factors, including the high antigen specificity of our αGPC3 mAb, high antigen expression by the HepG2 cells, and the absence of GPC3 in nontumor tissues. Because of the specificity of our antibody to human GPC3, the high signal contrast could potentially be due to failure of the antibody to bind to mouse GPC3 in native liver tissue, thus falsely elevating the tumor-to-liver ratio. Although this is a theoretic concern, multiple studies have demonstrated the specificity of GPC3 in tumor cells and absence in normal tissues (23–25), suggesting that this high contrast level would be possible in human subjects.

Additionally, orthotopic xenografts appear to exhibit higher tissue uptake than do flank xenografts when an identical cell line is used, likely because of a combination of optimized vascular anatomy and supportive hepatic tumor microenvironment, further highlighting a strength of the orthotopic model (Supplemental Fig. 2). The animal with the smaller hepatic tumor (<1 mm) demonstrated lower tissue uptake that was consistent with ^{89}Zr-PET studies reported by other investigators. This lower activity could be attributed to decreased ^{89}Zr-αGPC3 delivery by an underdeveloped angiogenic tumor blood supply and to underestimation of absolute radiotracer uptake in the tumor because of the partial-volume effect, which is caused by the finite spatial resolution of the PET imaging system (35). Given the promising targeting ability exhibited by αGPC3 in this study for use in imaging, conjugation to the therapeutic radioisotopes ^{90}Y, ^{211}At, and ^{177}Lu—all with readily available chelators for conjugation to αGPC3—is being studied. Additionally, preliminary studies indicate that in vitro, αGPC3 is internalized by HCC cells within 24 h, potentially enabling its use in drug delivery.

^{89}Zr-based immuno-PET imaging is a rapidly developing technology that has been used for anatomic detection of tumors (16,17), evaluation of immune modulation in atherosclerosis (36), and quantification of functional gene expression in malignancy (37). There is an increasing body of literature reporting on the application of immuno-PET in monitoring or validating treatment effect (36,38). This is the first reported application of ^{89}Zr-based PET imaging in primary HCC, overcoming the inherent limitations of this technology for liver imaging. Given the relatively long half-life of ^{89}Zr, radiation exposure in subjects undergoing immuno-PET must be considered. However, clinical trials on patients with breast cancer and patients with head and neck cancer have shown that ^{89}Zr can be used in PET at acceptable radiation doses (15,39). Use of F(ab′)2 to reduce blood half-life, enhance clearance, and reduce radiation exposure is being evaluated. Although careful dosimetry for αGPC3 is still ongoing, this approach has been feasible with other mAbs and therefore acceptable radiation doses should be achievable with this probe.

Ultimately, ^{89}Zr-αGPC3 immuno-PET may serve as an adjunct when traditional multiphase CT and MR are inconclusive about the identity of a hepatic lesion. Additionally, this

NIH-PA Author Manuscript

NIH-PA Author Manuscript

NIH-PA Author Manuscript

technology may enable the identification of extrahepatic metastases, thus potentially altering a patient's eligibility for transplantation or hepatectomy. As new mAb therapies are developed, ^{89}Zr-αGPC3 may also enable noninvasive identification of the GPC3 expression status of a tumor, as well as its response to therapy, without biopsy. Attempts to enhance sensitivity through the use of antibody fragments and tumor-internalizing adjuncts are ongoing. These approaches aim to improve signal-to-noise ratio by increasing radioconjugate delivery to the tumor and consequently minimizing overall radiation exposure.

CONCLUSION

This preclinical study represents the first reported use of ^{89}Zr-PET to image HCC. It demonstrated the ability of ^{89}Zr-αGPC3 to specifically localize HCC tumors in the liver with high signal-to-noise ratio and to noninvasively determine the GPC3-expression status of a lesion. With further study, ^{89}Zr-αGPC3 may alter an HCC patient's clinical course by more clearly identifying intra- and extrahepatic lesions, noninvasively determining the antigen expression profile of a tumor, and allowing clinicians to determine the most appropriate treatment at an earlier stage.

Supplementary Material

Refer to Web version on PubMed Central for supplementary material.

Acknowledgments

We thank Gregory Garwin and Barbara Lewellen for technical assistance with the small-animal PET studies.

References

1. Ferenci P, Fried M, Labrecque D, et al. Hepatocellular carcinoma (HCC): a global perspective. J Clin Gastroenterol. 2010; 44:239–245. [PubMed: 20216082]
2. Ferlay, J.; Soerjomataram, I.; Ervik, M., et al. [Accessed March 6, 2014] GLOBOCAN 2012: estimated cancer incidence, mortality and prevalence worldwide in 2012. International Agency for Research on Cancer website. http://globocan.iarc.fr
3. Bruix J, Sherman M. Practice Guidelines Committee, American Association for the Study of Liver Diseases. Management of hepatocellular carcinoma. Hepatology. 2005; 42:1208–1236. [PubMed: 16250051]
4. Ayyappan AP, Jhaveri KS. CT and MRI of hepatocellular carcinoma: an update. Expert Rev Anticancer Ther. 2010; 10:507–519. [PubMed: 20397916]
5. Sangiovanni A, Manini MA, Iavarone M, et al. The diagnostic and economic impact of contrast imaging techniques in the diagnosis of small hepatocellular carcinoma in cirrhosis. Gut. 2010; 59:638–644. [PubMed: 19951909]
6. Colli A, Fraquelli M, Casazza G, et al. Accuracy of ultrasonography, spiral CT, magnetic resonance, and alpha-fetoprotein in diagnosing hepatocellular carcinoma. Am J Gastroenterol. 2006; 101:513–523. [PubMed: 16542288]
7. Golfieri R, Marini E, Bazzocchi A, et al. Small (<or=3 cm) hepatocellular carcinoma in cirrhosis: the role of double contrast agents in MR imaging vs. multi-detector-row CT. Radiol Med (Torino). 2009; 114:1239–1266. [PubMed: 19697104]
8. Saborido BP, Diaz JC, de Los Galanes SJ, et al. Does preoperative fine needle aspiration-biopsy produce tumor recurrence in patients following liver transplantation for hepatocellular carcinoma? Transplant Proc. 2005; 37:3874–3877. [PubMed: 16386569]

NIH-PA Author Manuscript

NIH-PA Author Manuscript

NIH-PA Author Manuscript

9. Silva MA, Hegab B, Hyde C, Guo B, Buckels JA, Mirza DF. Needle track seeding following biopsy of liver lesions in the diagnosis of hepatocellular cancer. Gut. 2008; 57:1592–1596. [PubMed: 18669577]
10. Hayashi PH, Trotter JF, Forman L, et al. Impact of pretransplant diagnosis of hepatocellular carcinoma on cadaveric liver allocation in the era of MELD. Liver Transpl. 2004; 10:42–48. [PubMed: 14755776]
11. Bruix J, Llovet JM. Major achievements in hepatocellular carcinoma. Lancet. 2009; 373:614–616. [PubMed: 19231618]
12. Lu X, Zhao H, Yang H, et al. A prospective clinical study on early recurrence of hepatocellular carcinoma after hepatectomy. J Surg Oncol. 2009; 100:488–493. [PubMed: 19653238]
13. Kaur S, Venktaraman G, Jain M, Senapati S, Garg PK, Batra SK. Recent trends in antibody-based oncologic imaging. Cancer Lett. 2012; 315:97–111. [PubMed: 22104729]
14. Zhang Y, Hong H, Cai W. PET tracers based on zirconium-89. Curr Radiopharm. 2011; 4:131–139. [PubMed: 22191652]
15. Dijkers EC, Oude Munnink TH, Kosterink JG, et al. Biodistribution of ^{89}Zr-trastuzumab and PET imaging of HER2-positive lesions in patients with meta-static breast cancer. Clin Pharmacol Ther. 2010; 87:586–592. [PubMed: 20357763]
16. Nayak TK, Garmestani K, Milenic DE, Brechbiel MW. PET and MRI of metastatic peritoneal and pulmonary colorectal cancer in mice with human epidermal growth factor receptor 1-targeted ^{89}Zr-labeled panitumumab. J Nucl Med. 2012; 53:113–120. [PubMed: 22213822]
17. Ruggiero A, Holland JP, Hudolin T, et al. Targeting the internal epitope of prostate-specific membrane antigen with ^{89}Zr-7E11 immuno-PET. J Nucl Med. 2011; 52:1608–1615. [PubMed: 21908391]
18. Niu G, Li Z, Xie J, Le QT, Chen X. PET of EGFR antibody distribution in head and neck squamous cell carcinoma models. J Nucl Med. 2009; 50:1116–1123. [PubMed: 19525473]
19. Nayak TK, Garmestani K, Baidoo KE, Milenic DE, Brechbiel MW. Preparation, biological evaluation, and pharmacokinetics of the human anti-HER1 monoclonal antibody panitumumab labeled with ^{86}Y for quantitative PET of carcinoma. J Nucl Med. 2010; 51:942–950. [PubMed: 20484421]
20. Nayak TK, Garmestani K, Milenic DE, Baidoo KE, Brechbiel MW. HER1-targeted 86Y-panitumumab possesses superior targeting characteristics than ^{86}Y-cetuximab for PET imaging of human malignant mesothelioma tumors xenografts. PLoS ONE. 2011; 6:e18198. [PubMed: 21464917]
21. Ho M, Kim H. Glypican-3: a new target for cancer immunotherapy. Eur J Cancer. 2011; 47:333–338. [PubMed: 21112773]
22. Pilia G, Hughes-Benzie RM, MacKenzie A, et al. Mutations in GPC3, a glypican gene, cause the Simpson-Golabi-Behmel overgrowth syndrome. Nat Genet. 1996; 12:241–247. [PubMed: 8589713]
23. Hsu HC, Cheng W, Lai PL. Cloning and expression of a developmentally regulated transcript MXR7 in hepatocellular carcinoma: biological significance and temporospatial distribution. Cancer Res. 1997; 57:5179–5184. [PubMed: 9371521]
24. Capurro M, Wanless IR, Sherman M, et al. Glypican-3: a novel serum and histochemical marker for hepatocellular carcinoma. Gastroenterology. 2003; 125:89–97. [PubMed: 12851874]
25. Jia HL, Ye QH, Qin LX, et al. Gene expression profiling reveals potential biomarkers of human hepatocellular carcinoma. Clin Cancer Res. 2007; 13:1133–1139. [PubMed: 17317821]
26. Nakatsura T, Yoshitake Y, Senju S, et al. Glypican-3, overexpressed specifically in human hepatocellular carcinoma, is a novel tumor marker. Biochem Biophys Res Commun. 2003; 306:16–25. [PubMed: 12788060]
27. Park JO, Stephen Z, Sun C, et al. Glypican-3 targeting of liver cancer cells using multifunctional nanoparticles. Mol Imaging. 2011; 10:69–77. [PubMed: 21303616]
28. Wayner EA, Hoffstrom BG. Development of monoclonal antibodies to integrin receptors. Methods Enzymol. 2007; 426:117–153. [PubMed: 17697883]

NIH-PA Author Manuscript

NIH-PA Author Manuscript

NIH-PA Author Manuscript

29. Vosjan MJ, Perk LR, Visser GW, et al. Conjugation and radiolabeling of mono-clonal antibodies with zirconium-89 for PET imaging using the bifunctional chelate p-isothiocyanatobenzyl-desferrioxamine. Nat Protoc. 2010; 5:739–743. [PubMed: 20360768]
30. Gage GJ, Kipke DR, Shain W. Whole animal perfusion fixation for rodents. J Vis Exp. 2012:e3564.
31. Schaefer JV, Pluckthun A. Transfer of engineered biophysical properties between different antibody formats and expression systems. Protein Eng Des Sel. 2012; 25:485–506. [PubMed: 22763265]
32. De Cat B, David G. Developmental roles of the glypicans. Semin Cell Dev Biol. 2001; 12:117–125. [PubMed: 11292377]
33. Filmus J, Capurro M, Rast J. Glypicans. Genome Biol. 2008; 9:224. [PubMed: 18505598]
34. Filmus J, Selleck SB. Glypicans: proteoglycans with a surprise. J Clin Invest. 2001; 108:497–501. [PubMed: 11518720]
35. Soret M, Bacharach SL, Buvat I. Partial-volume effect in PET tumor imaging. J Nucl Med. 2007; 48:932–945. [PubMed: 17504879]
36. Majmudar MD, Yoo J, Keliher EJ, et al. Polymeric nanoparticle PET/MR imaging allows macrophage detection in atherosclerotic plaques. Circ Res. 2013; 112:755–761. [PubMed: 23300273]
37. Holland JP, Evans MJ, Rice SL, Wongvipat J, Sawyers CL, Lewis JS. Annotating MYC status with ^{89}Zr-transferrin imaging. Nat Med. 2012; 18:1586–1591. [PubMed: 23001181]
38. Janjigian YY, Viola-Villegas N, Holland JP, et al. Monitoring afatinib treatment in HER2-positive gastric cancer with ^{18}F-FDG and ^{89}Zr-trastuzumab PET. J Nucl Med. 2013; 54:936–943. [PubMed: 23578997]
39. Börjesson PKE, Jauw YWS, de Bree R, et al. Radiation dosimetry of ^{89}Zr-labeled chimeric monoclonal antibody U36 as used for immuno-PET in head and neck cancer patients. J Nucl Med. 2009; 50:1828–1836. [PubMed: 19837762]

NIH-PA Author Manuscript

NIH-PA Author Manuscript

NIH-PA Author Manuscript

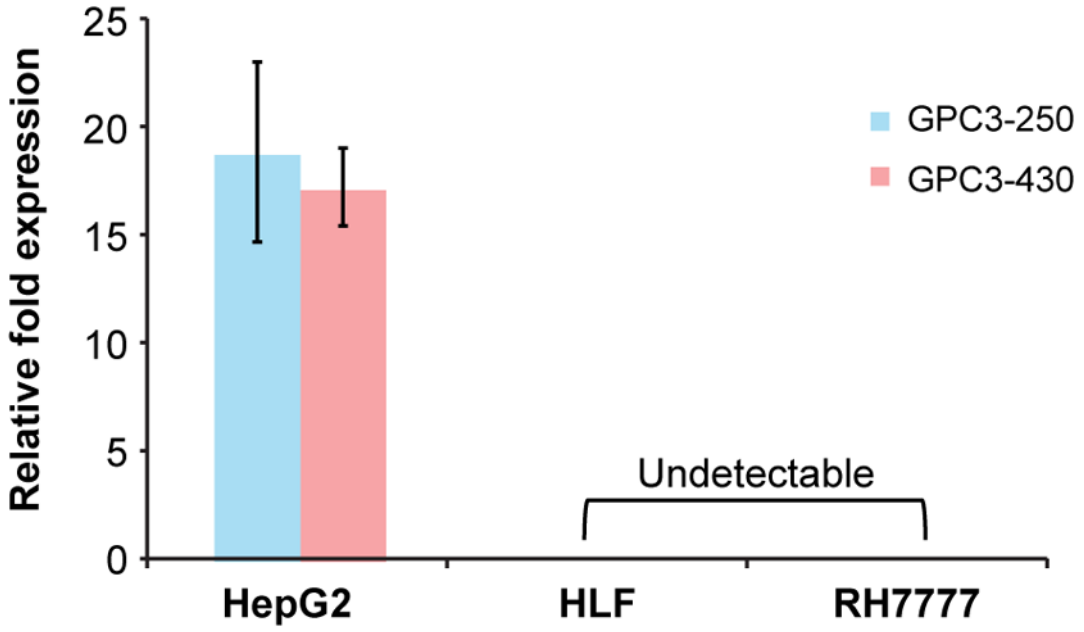

FIGURE 1.

Quantitative real-time polymerase chain reaction data demonstrating GPC3 expression relative to GAPDH across multiple cell lines verified by 2 nonoverlapping primer pairs.

NIH-PA Author Manuscript
NIH-PA Author Manuscript
NIH-PA Author Manuscript

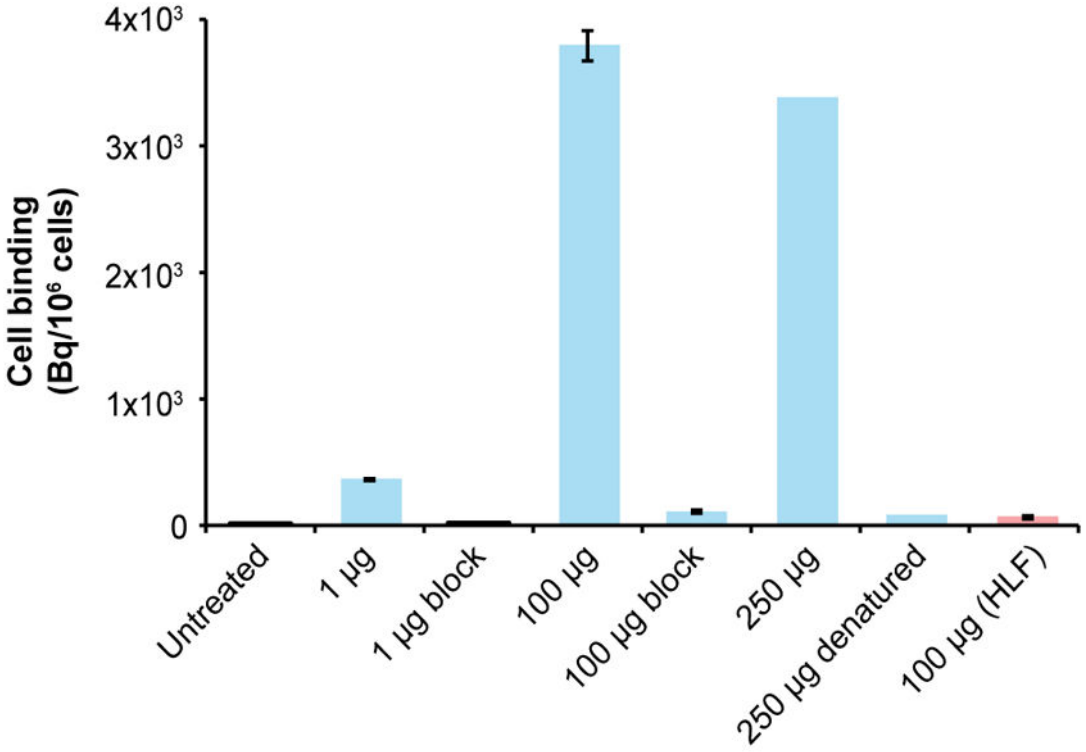

FIGURE 2.

In vitro binding of ^{89}Zr-αGPC3 after 1 h of treatment. All results are in HepG2 cells except final column (HLF).

NIH-PA Author Manuscript
NIH-PA Author Manuscript
NIH-PA Author Manuscript

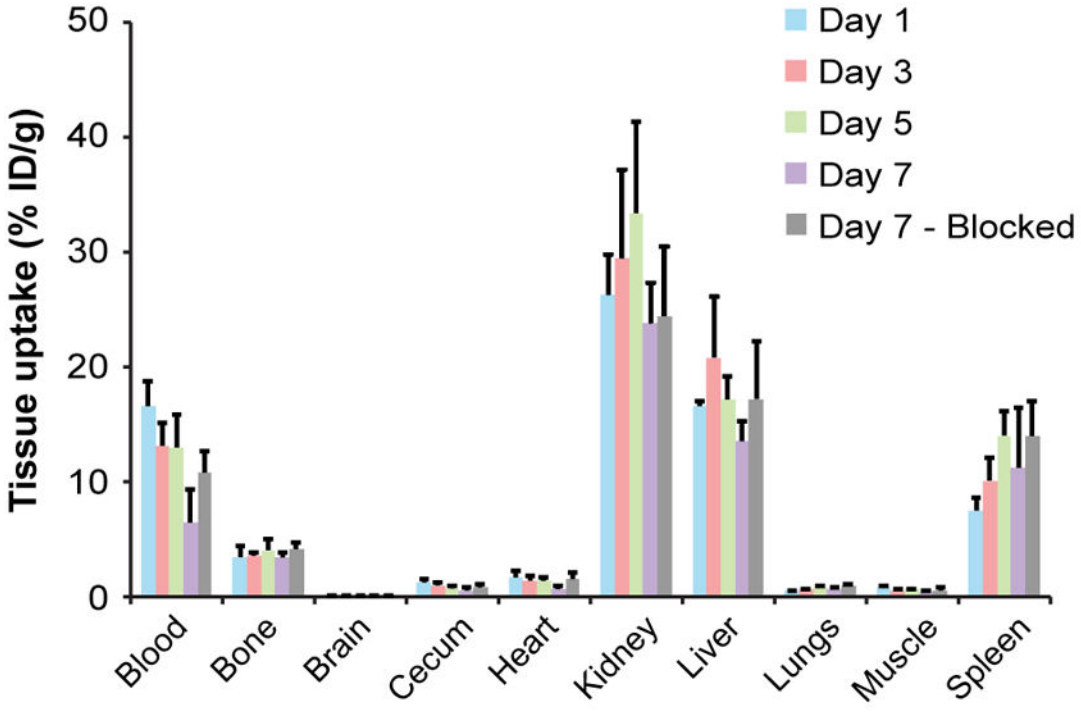

FIGURE 3.

Tissue biodistribution measured by Cobra II γ counter in non–tumor-bearing 8-wk-old female Nu/J mice (*n* = 4 each). Blocking was performed with 1.0–1.2 mg of unlabeled αGPC3.

NIH-PA Author Manuscript

NIH-PA Author Manuscript

NIH-PA Author Manuscript

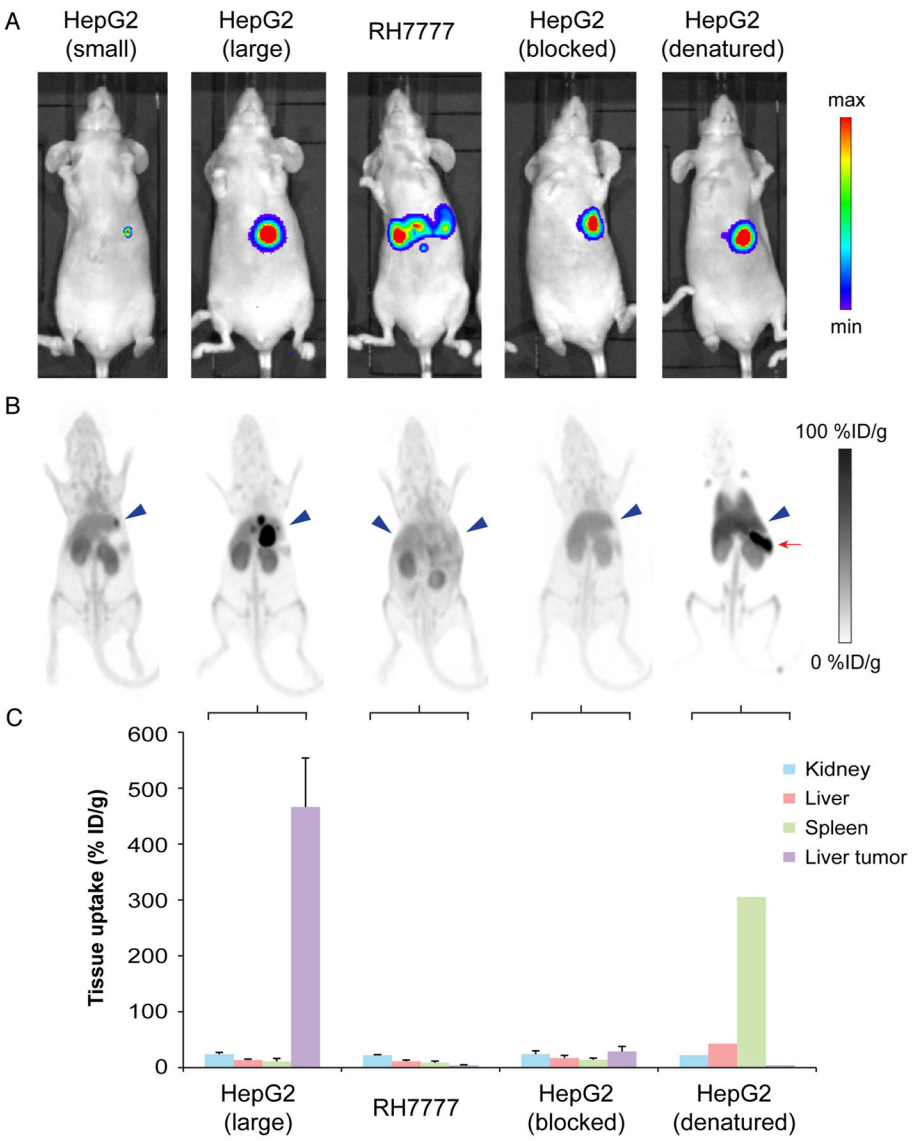

FIGURE 4.

(A) IVIS luminescent images before administration of ^{89}Zr-αGPC3. (B) Selected small-animal PET images of same animals showing tumor concordance in HepG2 tumor-bearing animals and lack of tumor uptake in RH7777, blocked, and heat-denatured controls. Signal saturation was permitted to enable comparisons between animals. Blue arrowheads indicate tumor location; red arrow indicates spleen. (C) Day 7 decay-corrected biodistribution of ^{89}Zr-αGPC3 confirming low liver tumor uptake in RH7777, blocked, and heat-denatured controls.

NIH-PA Author Manuscript

NIH-PA Author Manuscript

NIH-PA Author Manuscript

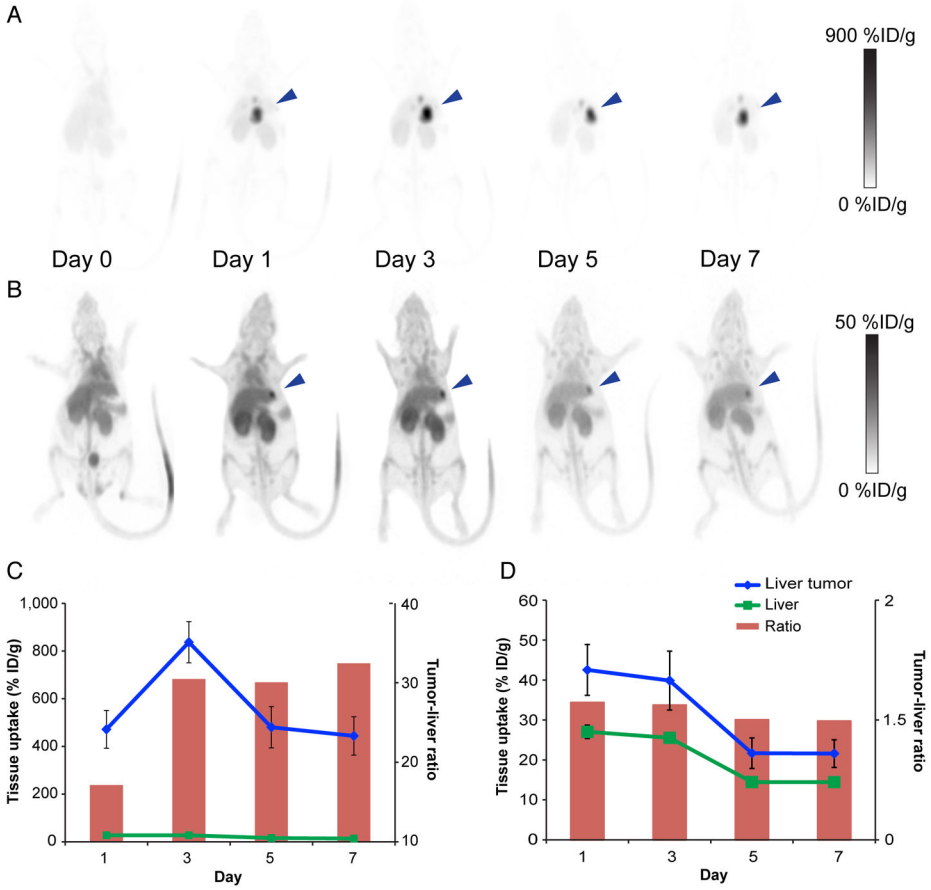

FIGURE 5.

(A and B) Serial decay-corrected whole-body small-animal PET images of mouse bearing large HepG2 tumor (3.8 mm) (A) and small HepG2 tumor (<1 mm) (B). Blue arrowhead indicates tumor location. (C and D) Average tumor and liver activity obtained from small-animal PET data for mouse with large HepG2 tumor (C) and mouse with small HepG2 tumor (D).

NIH-PA Author Manuscript
NIH-PA Author Manuscript
NIH-PA Author Manuscript

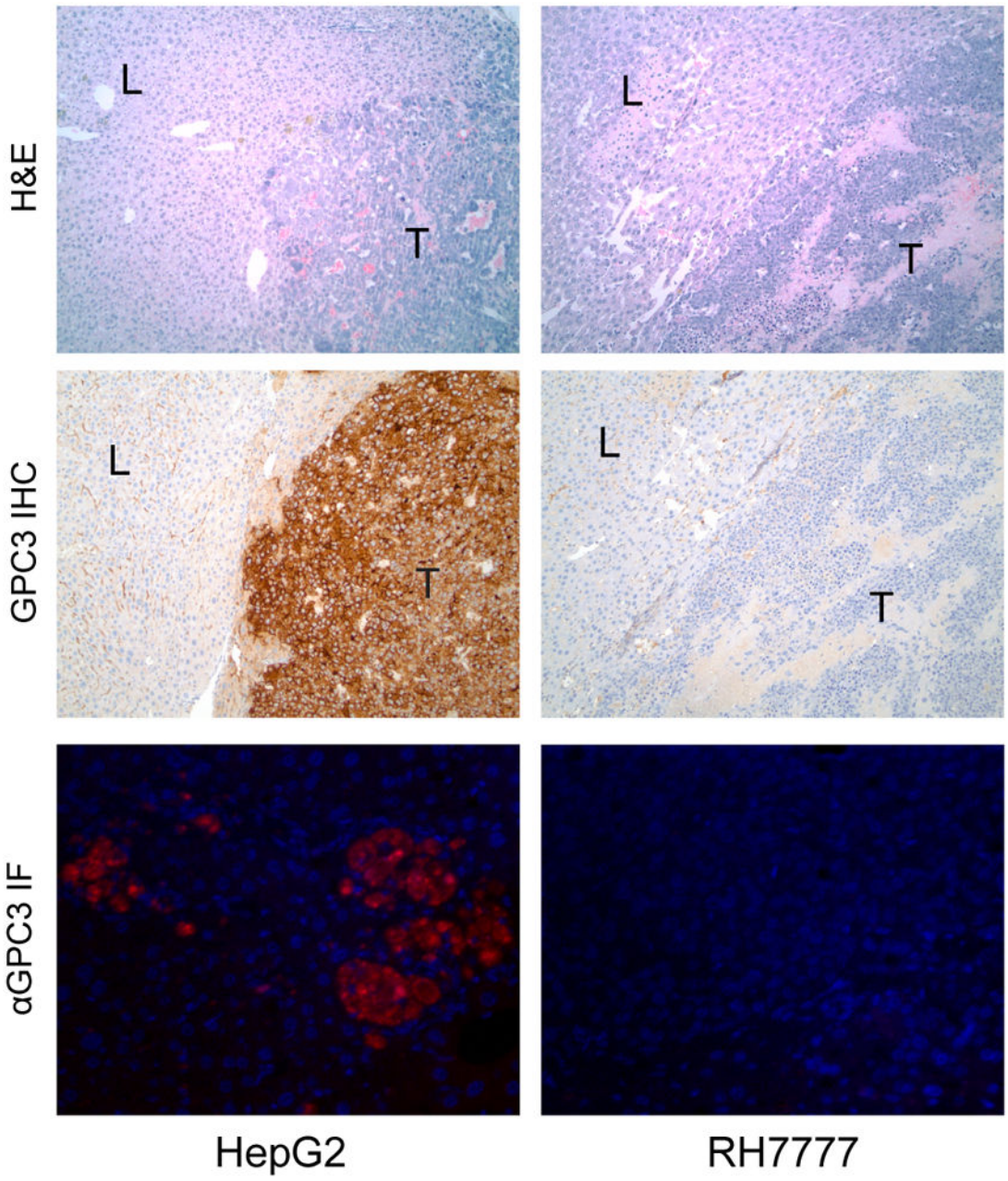

FIGURE 6.

Histologic sections of PET-imaged mouse liver (L) and liver tumor (T) stained with hematoxylin and eosin (top row) and immunohistochemistry against GPC3 (middle row) viewed at ×100 magnification. Immunohistochemistry confirms polymerase chain reaction data showing high expression in HepG2 and minimal expression in RH7777 tumors. Bottom row demonstrates immunofluorescence of goat antimouse secondary antibody binding against mouse antihuman αGPC3 in HepG2 and RH7777 tumors.